

1 **Suppression of MDA5-mediated antiviral immune responses by NSP8 of SARS-CoV-2**

2

3

4 Running title: SARS-CoV-2 NSP8 suppresses MDA5-mediated antiviral responses

5

6

7 Ziwei Yang^{1,2}, Xiaolin Zhang¹, Fan Wang¹, Peihui Wang³, Ersheng Kuang^{1,2,*} and Xiaojuan Li^{1,2,*}

8

9

10 ¹ Institute of Human Virology, Zhongshan School of Medicine, Sun Yat-Sen University, Guangzhou,
11 Guangdong, 510080, China

12 ² Key Laboratory of Tropical Disease Control (Sun Yat-Sen University), Ministry of Education,
13 Guangzhou, Guangdong, 510080, China

14 ³ Advanced Medical Research Institute, Shandong University, Jinan, Shandong 250012, China

15

16

17 * Correspondence: Xiaojuan Li, E-mail: lixjuan3@mail.sysu.edu.cn and Ersheng Kuang, E-mail:
18 kuangersh@mail.sysu.edu.cn, Zhongshan School of Medicine, Sun Yat-sen University North Campus,
19 74 Zhongshan 2nd Rd, Guangzhou, 510080, China;

20

21

22

23

24

25

26 **Abstract**

27 Melanoma differentiation-associated gene-5 (MDA5) acts as a cytoplasmic RNA sensor to detect viral
28 dsRNA and mediates type I interferon (IFN) signaling and antiviral innate immune responses to infection by
29 RNA viruses. Upon recognition of viral dsRNA, MDA5 is activated with K63-linked polyubiquitination and then
30 triggers the recruitment of MAVS and activation of TBK1 and IKK, subsequently leading to IRF3 and NF- κ B
31 phosphorylation. Great numbers of symptomatic and severe infections of SARS-CoV-2 are spreading
32 worldwide, and the poor efficacy of treatment with type I interferon and antiviral agents indicates that SARS-
33 CoV-2 escapes from antiviral immune responses via an unknown mechanism. Here, we report that SARS-
34 CoV-2 nonstructural protein 8 (NSP8) acts as an innate immune suppressor and inhibits type I IFN signaling
35 to promote infection of RNA viruses. It downregulates the expression of type I IFNs, IFN-stimulated genes and
36 proinflammatory cytokines by binding to MDA5 and impairing its K63-linked polyubiquitination. Our findings
37 reveal that NSP8 mediates innate immune evasion during SARS-CoV-2 infection and may serve as a potential
38 target for future therapeutics for SARS-CoV-2 infectious diseases.

39

40

41 **Importance**

42 The large-scale spread of COVID-19 is causing mass casualties worldwide, and the failure of antiviral
43 immune treatment suggests immune evasion. It has been reported that several nonstructural proteins of
44 severe coronaviruses suppress antiviral immune responses; however, the immune suppression mechanism
45 of SARS-CoV-2 remains unknown. Here, we revealed that NSP8 protein of SARS-CoV-2 directly blocks the
46 activation of the cytosolic viral dsRNA sensor MDA5 and significantly downregulates antiviral immune
47 responses. Our study contributes to our understanding of the direct immune evasion mechanism of SARS-
48 CoV-2 by showing that NSP8 suppresses the most upstream sensor of innate immune responses involved in
49 the recognition of viral dsRNA.

50

51 **Key words:**

52 SARS-CoV-2, NSP8, MDA5, interferon, immune evasion

53 Introduction

54 Severe acute respiratory syndrome coronavirus 2 (SARS-CoV-2) is an emerging severe coronavirus that is
55 currently causing a global outbreak of Coronavirus Disease 2019 (COVID-19). It has infected more than twenty
56 million patients and caused more than two-thirds of a million deaths. The number of patients and deaths are
57 still rapidly increasing; however, no effective therapy, vaccine or cure are available. Knowledge of SARS-CoV-
58 2 infection, pathogenesis, diseases and treatments remains limited, and novel targets of therapeutics and
59 drug development are quite urgently needed.

60 Analysis of clinical data from different SARS-CoV-2 patients has shown that excessive cytokine release,
61 known as a “cytokine storm”, is closely related to disease severity ¹⁻³. To characterize the host immune and
62 inflammatory responses in COVID-19 patients, genome-wide RNA-sequencing analysis was performed, which
63 indicated that the proportion of immune cells in the blood was reduced in patients who required non-ICU
64 admission, with lower levels of *GCSF*, *CXCL10/IP-10*, *CCL2/MCP-1* and *CCL3/MIP-1A* detected. In addition,
65 some anti-inflammatory cytokines, such as IL-10 and TGF- β , were found to be induced during SARS-CoV-2
66 infection ⁴. Accordingly, compared with ICU care patients, non-ICU care patients had lower plasma levels of
67 cytokines, including IL-2, IL-7, IL-10, GSCF, IP10, MCP1, MIP1A, and TNF α . Furthermore, mild cases of
68 COVID-19 exhibited decreased plasma levels of IL2R and IL6 compared with severe cases, while an
69 excessive inflammatory response was observed in dead cases ^{5,6}. These studies reported a correlation
70 between the release of inflammatory cytokines and pathogenesis of SARS-CoV-2.

71 SARS-CoV-2 and other coronaviruses generate massive amounts of RNA products during their infection
72 that are then recognized by host cytosolic RNA sensors, including retinoic acid-inducible gene I (RIG-I) and
73 melanoma differentiation-associated gene-5 (MDA5) ⁷. Activation of RIG-I and MDA5 triggers the formation of
74 signalosomes that induce the expression of type I IFN and ISGs and the subsequent execution of an antiviral
75 state within the cell ⁸. To escape immune elimination and to survive and then replicate, coronaviruses, including
76 SARS-CoV and MERS-CoV, have evolved strategies to inhibit or delay IFN production and responses. SARS-
77 CoV encodes a set of accessory proteins, several of which target the innate immune response. Its
78 nonstructural protein 1 (NSP1) binds to the 40S ribosome to inactivate translation and induces host mRNA
79 degradation ^{9,10}; NSP15 was identified as an IFN antagonist to enhance immune evasion ^{11,12}; NSP16, a 2'O-

80 methyltransferase (2'O-MTase), provides a cap structure at the 5'-end of viral mRNAs to evade MDA5
81 detection¹³⁻¹⁵; furthermore, open reading frame 6 (ORF6) also reduces IFN production¹⁶. In addition, ORF-
82 9b localizes to mitochondrial membranes to induce the degradation of MAVS, TRAF3 and TRAF6, severely
83 limiting host cell IFN production¹⁷. In addition, MERS ORF4b is involved in evasion of the innate immune
84 response by binding α -karyopherin proteins, leading to the inhibition of NF- κ B nuclear translocation¹⁸.

85 Considering the numerous existing asymptomatic infected populations, it is reasonable to suggest that
86 SARS-CoV-2 has evolved effective strategies to inhibit the host immune response, which is also a challenge
87 for preventing and treating COVID-19. Consistent with these observations, a recent study showed that NSP1
88 of SARS-CoV-2 shuts down host mRNA translation by binding to 40S and 80S ribosomes, effectively blocking
89 RIG-I-dependent innate immune responses¹⁹. However, the potential immune inhibitory mechanism mediated
90 by viral components of SARS-CoV-2 is not well known.

91 We performed a systematic screening and determined that SARS-CoV-2 NSP8 is a suppressor of the type
92 I immune response upon RNA viral infection. It decreases type I IFN production and ISG expression, by which
93 it interacts with the MDA5 CARD domain and then inhibits MDA5 K63-linked polyubiquitination and thus
94 terminates MDA5-mediated immune responses.

95

96 **Results**

97 **NSP8 inhibits viral RNA-related type I interferon and antiviral responses.**

98 To investigate a factor of SARS-CoV-2 that suppresses the type I IFN signaling pathway, we screened a
99 panel of viral nonstructural proteins (NSPs) that regulate the expression of interferon and inflammatory factors
100 using RT-PCR arrays. 293T cells were transfected with empty vector or NSP-expressing plasmids for 24 h.
101 The cells were left untreated or challenged with dsRNA analog poly(I:C) for 18 h or 24 h separately and then
102 harvested for analysis of gene expression. Several NSPs exhibited the inhibitory effects on immune and
103 inflammatory gene expression (Supplementary Fig.1). We found that NSP8 significantly downregulated the
104 expression of *TNF- α* , *IFN- β* , interferon-stimulated genes (ISGs) *IFIT1* and *IFIT2* and proinflammatory
105 cytokines *IL-6* and *CCL-20* (Fig.1a). Consistent with our results, NSP1 was previously reported to inhibit the
106 translation of type I interferon to evade the immune response, which validated our screening approach^{9,19}.

107 To confirm that the attenuation of the type I IFN response by NSP8 is correlated with a decrease in the
108 antiviral response, *NSP8*-overexpressing 293T cells were subsequently infected with vesicular stomatitis virus
109 tagged with enhanced GFP (VSV-eGFP). As analyzed by fluorescence microscopy and flow cytometry, NSP8
110 overexpression increased the percentage of GFP-positive cells with the extended response time compared
111 with empty vector-transfected cells (Fig.1b,c), suggesting that NSP8 promoted the efficiency of viral infection
112 and gene expression, hence favoring VSV-eGFP replication. These data demonstrated that NSP8 is an
113 inhibitory protein in type I IFN signaling and antiviral responses during SARS-CoV-2 infection.

114

115 **NSP8 decreases MAVS-dependent antiviral responses.**

116 To further understand whether the inhibitory effects of NSP8 are exerted on both the IRF3 and NF- κ B
117 pathways, 293T cells were cotransfected with empty vector or IRF3 or p65 expressing plasmid and with NSP8-
118 expressing plasmid, followed by VSV infection for the indicated time points. By immunoblotting analysis to
119 detect the effect of NSP8 on the phosphorylation of TBK1 (pTBK1), the phosphorylation of IRF3 (pIRF3)
120 (Fig.2a), the phosphorylation of IKK α/β (pIKK α/β), the phosphorylation of p65 (p-p65) and I κ B α (Fig.2b), we
121 found that in NSP8-overexpressing cells, pTBK1 level was four- to nine-fold lower than that in control cells
122 after VSV infection. As a downstream transcription factor that is phosphorylated and activated by TBK1, IRF3
123 phosphorylation was entirely blocked in NSP8-overexpressing cells (Fig.2a). Similarly, inhibition of IKK α/β
124 phosphorylation by NSP8 led to the stabilization of I κ B α , and NF- κ B signaling was strongly inhibited by NSP8
125 overexpression, as indicated by the decrease in p65 phosphorylation (Fig.2b). These results confirm that
126 NSP8 suppresses the activation of both IRF3 and NF κ B and the upstream cascade of the type I IFN signaling
127 pathway.

128 To investigate whether NSP8 plays a role in the early step of the type I IFN signaling cascade, we detected
129 the inhibitory effect of NSP8 in MAVS-deficient vs. complemented cells. *MAVS* knockout HEK293T cells
130 (HEK293T^{MAVS^{-/-}}) were cotransfected with *NSP8*-expressing plasmid or empty vector and with *MAVS*-
131 expressing plasmid or empty vector and then stimulated with poly(I:C) for different times. As expected, the
132 expression of *TNF- α* , *IFN- β* , *IFIT1*, *IFIT2*, *IL-6* and *CCL-20* was not downregulated by NSP8 upon stimulation
133 (Fig.2c, black vs. white columns), while MAVS overexpression in HEK293T^{MAVS^{-/-}} cells significantly restored

134 their induction upon stimulation, and NSP8 once again had suppressive effects on the expression of these
135 cytokines (Fig.2c, red vs. blue columns). Taken together, these results suggest that NSP8 suppresses MAVS-
136 dependent innate immune responses, probably by acting on either MAVS or upstream RNA sensors.

137

138 **NSP8 interacts with MDA5 and suppresses MDA5 K63-linked polyubiquitination**

139 Since viral RNA of coronaviruses contains a methylated 5'-cap and 3'-polyA tail that is similar to cellular
140 mRNA, we assumed that NSP8 may preferentially regulate MDA5-mediated responses rather than RIG-I-
141 mediated responses that recognize 5'-pppRNA. Hence, we performed coimmunoprecipitation (co-IP) analysis
142 and found that NSP8 interacts with MDA5 (Fig.3a). Furthermore, we mapped the binding domain and
143 determined that its CARD domain is responsible for the NSP8 interaction (Fig.3b). As a result, MDA5-mediated
144 ISRE-luc activity was inhibited by NSP8 in a dose-dependent manner (Fig.3c). In addition, confocal
145 microscopy demonstrated that NSP8 tightly colocalized with MDA5 inside cells (Fig.3d). These results suggest
146 that NSP8 interacts with MDA5 and directly suppresses MDA5-mediated immune responses.

147 To further understand the molecular mechanism by which NSP8 interacts and interferes with MDA5, we
148 predicted the MDA5 CARD, NSP8 and K63-Ub tertiary structures with SWISS-MODEL, and then the predicted
149 structures were input into ZDOCK SERVER for simulation. Predicted docking models were processed in
150 PyMOL for visualization. Surprisingly, we found that NSP8 possesses a long α -helix (Supplementary Fig.2a),
151 which is tightly packed in the ravines formed by the two α -helices of MDA5 CARDS. The random coil and a
152 short α -helix in the N terminus of NSP8 occupy the area or space that interacts with K63-Ub (Fig.3e and
153 Supplementary Fig.2b). Further calculation of vacuum electrostatics for this binding model demonstrated that
154 the contact area in the chain of MDA5 CARDS is positively charged, while the corresponding area in the chain
155 of NSP8 is negatively charged (Fig.3f and Supplementary Fig.2c), implying that there is a likely interaction of
156 these two structures. We further searched the polar contacts in the interface of the binding model with PyMOL
157 and found that 7 paired residues anchor with each other, one locates in the N-terminal coil of NSP8 while the
158 others are in the long α -helix (Fig.3g). Thus, computer-based molecular structural prediction and modeling
159 implies that NSP8 interacts with the MDA5 CARD domain probably through ionic interactions and dipolar
160 surfaces between the NSP8 and MDA5 CARD binding pockets.

161 Next, we sought to determine how NSP8 inhibits MDA5 activation. It is well documented that upon virus
162 infection, the MDA5 CARD domain undergoes K63-linked polyubiquitination and recruits MAVS to form a
163 signalosome²⁰. The structural prediction of the NSP8-MDA5 CARD interaction showed that NSP8 may
164 interrupt this process since it interacts with MDA5 at its CARD domain and shields the binding area or space
165 for K63-ubiquitin linkage (Fig.3e, Supplementary Fig.2, and pdb file). The polyubiquitination of MDA5 was
166 analyzed in the presence or absence of NSP8 expression. The *MDA5*-expressing plasmid was cotransfected
167 into HEK293T cells with a WT-, K48-, or K63-linked ubiquitin-expressing plasmid, and an in vivo ubiquitination
168 assay showed that MDA5 WT- and K63-linked polyubiquitination were strongly inhibited (Fig.4a,c), while K48-
169 linked polyubiquitination was barely affected (Fig.4b). Thus, these results reveal that NSP8 interferes with the
170 MDA5-MAVS signalosome by inhibiting the K63-linked polyubiquitination of MDA5.

171

172 **NSP8 decreases the expression of antiviral immune and inflammatory genes.**

173 Next, we investigated whether NSP8 affects the downstream expression of immune and inflammatory genes
174 and cytokines. NSP8-expressing A549 cells were collected, and total RNA was subjected to RT-PCR array
175 analysis for immune and inflammatory gene expression (Primer listed in Supplementary Table.1). The
176 expression of the majority of cytokines, including *IL-1 β* , *IL-2*, *IL-5*, *IL-6*, *IL-26*, *IL-33*, *IFN- β* , *IFIT1* and *IFIT2*,
177 was downregulated by NSP8 expression. The transcription of some pleiotropic chemoattractant cytokines,
178 such as *IL-16*, *IL-17A*, *IL-17F*, and *IL17C*, was also downregulated. Furthermore, a decreasing transcription
179 tendency was also observed for the inflammatory receptors *IL-1RI*, *IL-1RII*, *IL-2R α* , and *IL18RII*; NK cell-
180 associated activation receptors, such as *NKp44*, *NKp46*, and *NKG2B*; and the trans-acting T-cell-specific
181 transcription factor *GATA3* (Fig.5a), indicating that the activation of T cells and NK cells was attenuated by
182 NSP8 through the suppression of these key factors. Although these decreased cytokines and receptors may
183 not be directly activated by IRF3 or NF κ B, they could be regulated by downstream cytokines or other factors
184 derived from these two pathways. In contrast, the cytokine IL-2 and IFN-gamma suppression gene *FOXP3*
185 was significantly increased with NSP8 overexpression.

186 To further confirm that the downregulation of these immune and inflammatory cytokines and genes is
187 mediated by NSP8 under physiological conditions, A549 cells were transfected with an NSP8-expressing

188 plasmid or empty vector and then stimulated with poly(I:C) mimicking viral RNA for the indicated times. The
189 inhibition of the expression of key cytokines and related genes was verified, and NSP8 negatively regulated
190 the expression of these immune and inflammatory genes (Fig.5b). Collectively, these results suggest that
191 NSP8 could strongly impair the expression of genes involved in antiviral immune and inflammatory responses.

192

193 **Discussion**

194 It has not been well investigated whether SARS-CoV-2 components have immunosuppressive functions, so
195 we are very interested in exploring the roles of SARS-CoV-2 proteins, especially the nonstructural protein
196 family (NSP), in viral immune evasion. In the present study, we screened a panel of NSPs and identified NSP8
197 as an immune suppressor of the type I IFN signaling pathway. We have shown that NSP8 overexpression
198 impaired type I IFN production and the gene expression of immune and inflammatory factors, including *TNF-*
199 *α*, *IFN-β*, *IFIT1*, *IFIT2*, *IL-6* and *CCL-20*. As a consequence, we observed that VSV-eGFP infection was
200 significantly increased in cells with NSP8 overexpression. The subsequent detection of phosphorylation of
201 kinases TBK1 and IKK α / β and substrates IRF3 and p65 provided evidence that both IRF3 and NF κ B activity
202 were inhibited by NSP8. MAVS is an upstream regulator of the type I IFN signaling cascade and regulates
203 both pathways; hence, we overexpressed NSP8 in MAVS knockout HEK293T cells and observed that the
204 inhibitory function of NSP8 towards type I IFN and cytokines was completely abolished. Re-expressing MAVS
205 in MAVS KO HEK293T cells that also express NSP8 successfully restored the NSP8 inhibitory activity.
206 Consequently, a series of antiviral immune and inflammatory cytokines and related genes were further strongly
207 downregulated by NSP8 expression.

208 Herein, we speculated that NSP8 may act on RIG-I or MDA5, two upstream viral RNA sensors. Our results
209 showed that NSP8 directly interacted with MDA5 on its CARD domains, and MDA5-mediated type I IFN
210 signaling activities were strongly inhibited at the same time. Polyubiquitinated modification of MDA5 is crucial
211 for its antiviral responses, K48-linked polyubiquitination mediates MDA5 proteasomal degradation²¹, and K63-
212 linked polyubiquitination mediates MDA5-induced type I IFN expression²⁰. We speculated that NSP8 may
213 inhibit type I IFN signaling through the polyubiquitinated modification of MDA5. To test our hypothesis, we
214 determined the status of WT-, K48- and K63-linked polyubiquitination of MDA5 in the absence or presence of

215 NSP8 and confirmed that WT- and K63-linked polyubiquitination were impaired by NSP8, while K48-linked
216 polyubiquitination was barely changed. We therefore conclude that under certain circumstances, NSP8
217 jeopardizes antiviral responses by impairing MDA5 K63-linked polyubiquitination.

218 Based on our existing experimental data, we propose a simple working model to illustrate how NSP8
219 negatively regulates innate immune responses by inhibiting MDA5 K63-linked polyubiquitination (Fig.5c).
220 Upon SARS-CoV-2 infection, cytosolic viral dsRNA is recognized by MDA5 and triggers type I IFN expression;
221 meanwhile, NSP8 is largely expressed and localized in the cytoplasm of host cells and then interacts with
222 MDA5 on its CARD domains to inhibit its K63-linked polyubiquitination, consequently negatively regulating
223 type I IFN signaling and antiviral immune responses, thus favoring viral infection and replication.

224 Interestingly, a recent study showed that in the carrier and intermediate host of coronaviruses—pangolin—
225 the MDA5 gene is mutated and dysfunctional ²², while RIG-I and TLR 3, 7 and 8 are conserved among three
226 different species. Considering the coexisting relationship between pangolins and coronaviruses and the
227 tolerance of pangolins for SARS-CoV-2 infection, this finding implied that coronaviruses may be inclined to
228 silence MDA5-mediated innate immunity because they could generate more drastic reactivity and injury upon
229 viral RNA recognition. Based on this observation and the findings of our present study, the suppressive
230 function of NSP8 in antiviral responses and its impairment of MDA5 activation have been identified,
231 representing a direct immune evasion mechanism of the recognition of viral dsRNA.

232 Multiple posttranslational modifications, including phosphorylation, acetylation, methylation and
233 polyubiquitination, are employed to regulate the antiviral signalosome ²³. Among these modifications,
234 polyubiquitination is commonly used for the degradation or activation of MDA5 and RIG-I. The E3 ubiquitin
235 ligase TRIM40 targets MDA5 and RIG-I to promote their K27- and K48-linked ubiquitination, thus leading to
236 their proteasomal degradation for immune silencing, but upon RNA virus infection, TRIM40 is downregulated
237 to allow the activation of a sufficient antiviral immune response ²¹. Likewise, some viral proteins, such as
238 Epstein-Barr virus protein BPLF1, which has ubiquitin- and NEDD8-specific deconjugase activity, interact with
239 scaffold proteins 14-3-3 and TRIM25 to form a tri-molecular complex, consequently promoting the dimerization
240 and ubiquitination of TRIM25. Consequently, K63-linked polyubiquitination of RIG-I is downregulated, leading
241 to the attenuation of RIG-I-mediated type I IFN antiviral responses ²⁴. In addition, the NS3 protein of ZIKA virus

242 interacts with scaffold proteins 14-3-3 ϵ and η separately through its 14-3-3 binding motif, hence blocking the
243 translocation of RIG-I and MDA5 from the cytosol to mitochondria, impairing signalosome formation with MAVS,
244 and antagonizing innate immunity²⁵. Our studies revealed that NSP8 of SARS-CoV-2 acts as a binding partner
245 of MDA5 to shield its K63-linked polyubiquitination and then impairs the formation or activation of the MDA5
246 signalosome.

247 In summary, our study provides insights into the potential mechanisms of SARS-CoV-2 NSP8 in the
248 inhibition of type I IFN signaling and antiviral responses. We provide compelling evidence that NSP8 plays a
249 critical negative role in MDA5-mediated antiviral responses and demonstrate specific orchestration of the viral
250 dsRNA-triggered signalosome and signal cascade by NSP8. Importantly, considering that MDA5 plays a key
251 pathological role in antiviral immunity towards severe coronaviruses, antagonists of NSP8 could serve as a
252 promising therapeutic target for COVID-19 therapies.

253

254 **Materials and Methods**

255 Cell culture and antibodies

256 HEK293T cells were cultured in DMEM (Gibco) supplemented with 10% fetal bovine serum (FBS). A549
257 cells (human adenocarcinoma lung tissue-derived epithelial cells) were cultured in RPMI 1640 (Gibco) medium
258 containing 10% FBS. The following antibodies were used in this study: goat anti-mouse IRDye680RD
259 (C90710-09) and goat anti-rabbit IRDye800CW (C80925-05), which were purchased from Li-COR; anti-HA
260 (M132-3), purchased from MBL; anti-Flag (AE005), anti-GFP (AE0122) and anti-IRF3 (A2172), purchased
261 from ABclonal; anti- β -actin (HC201-01), purchased from TransGen; and anti-pTBK1 (#5483P), anti-TBK1
262 (#3504), anti-pIRF3 (#4947), anti-phospho-NF- κ B p65 (#3033), and anti-NF- κ B p65 (#8242), purchased from
263 Cell Signaling Technology.

264

265 Plasmids

266 The following plasmids were used. Flag-NSP8 was kindly provided by the Peihui Wang lab (Shandong
267 University). HA-tagged Ub, K48-Ub (K48 only), and K63-Ub (K63 only) were kindly provided by Dr Yang Du
268 (Sun Yat-Sen University). To generate GFP- and mCherry-tagged NSP8 and GFP- and Flag-tagged MDA5,

269 the NSP8 and MDA5 fragments were subcloned into the pEGFP-C2, p-mCherry-C2 and pcDNA3.1 vectors.

270

271 Transfection and luciferase reporter assays

272 HEK293T cells were seeded in 24-well plates overnight and then transfected using Lipofectamine 2000
273 (Invitrogen) with 100 ng ISRE luciferase reporter (firefly luciferase), 20 ng pRL-TK plasmid (Renilla luciferase),
274 150 ng Flag-MDA5 expressing plasmid and increasing amounts (0, 100, or 200 ng) of NSP8-expressing
275 plasmid. Twenty-four hours post transfection, cells were collected, and luciferase activity was measured with
276 a Dual-Luciferase Assay kit (Promega) with a Synergy2 Reader (Bio-Tek) according to the manufacturer's
277 protocol. The relative level of gene expression was determined by normalization of firefly luciferase activity to
278 Renilla luciferase activity.

279

280 Virus infection

281 VSV-eGFP was kindly provided by Dr Meng Lin, School of Life Sciences, Sun Yat-Sen University. Cells were
282 infected at various MOIs, as previously described ²⁶.

283

284 Real-time PCR

285 Total RNA was extracted using TRIzol reagent (Invitrogen) and subjected to reverse transcription using
286 HiScript® III RT SuperMix (Vazyme). Real-time PCR was performed with a LightCycler® 480 SYBR Green I
287 Master Mix kit (Roche). The primers used in the indicated gene array are listed in Table S1. The following
288 primers were used for real-time PCR:

289 *TNF α* :

290 Forward 5'-CTCTTCTGCCTGCTGCACTTTG-3'

291 Reverse 5'-ATGGGCTACAGGCTTGTCCTC-3'

292 *IFN β* :

293 Forward 5'-CCTACAAAGAAGCAGCAA-30-3'

294 Reverse 5'-TCCTCAGGGATGTCAAAG-30-3'

295 *IFIT1*:

296 Forward 5'-GCCTTGCTGAAGTGTGGAGGAA-3'

297 Reverse 5'-ATCCAGGCGATAGGCAGAGATC-3'

298 *IFIT2*:

299 Forward 5'-GGAGCAGATTCTGAGGCTTTGC-3'

300 Reverse 5'-GGATGAGGCTTCCAGACTCCAA-3'

301 *IL-6*:

302 Forward 5'-AGACAGCCACTCACCTCTTCAG-3'

303 Reverse 5'-TTCTGCCAGTGCCTCTTTGCTG-3'

304 *CCL20*:

305 Forward 5'-AAGTTGTCTGTGTGCGCAAATCC-3'

306 Reverse 5'-CCATTCCAGAAAAGCCACAGTTTT-3'

307

308 Immunoprecipitation and immunoblot analysis

309 For immunoprecipitation, whole cell extracts were prepared after transfection or stimulation with appropriate
310 ligands, followed by incubation for 1 h at 4°C with anti-GFP agarose beads (AlpaLife). Beads were washed 4
311 times with low-salt lysis buffer, and immunoprecipitants were eluted with 2x SDS loading buffer and then
312 resolved by SDS-PAGE. Proteins were transferred to PVDF membranes (Millipore) and further incubated with
313 the appropriate primary and secondary antibodies. The images were visualized using Odyssey Sa (LI-COR).

314

315 Computer-based prediction and structural modeling

316 NSP8.pdb, MDA5-CARDs.pdb and K63-Ub.pdb were generated in SWISS-MODEL ²⁷. MDA5-CARDs.pdb
317 was input into ZDOCK-SERVER ²⁸ as a receptor, while NSP8 or K63-Ub was input as a ligand for docking
318 computation. MDA5-CARDs with NSP8.pdb and MDA5-CARDs with K63-Ub.pdb were the best fit prediction
319 models chosen from the results. All the pdb files were processed and visualized with PyMOL (Schrödinger).

320

321

322 **Author contributions**

323 X.L. and E.K. initiated the concept. Z.Y., X.L. and E.K. designed the experiments and analyzed the data. P.W.
324 provided the reagents. Z.Y., X.Z., F.W. performed the experiments. Z.Y. and E.K. wrote the paper.

325

326

327 **Acknowledgments**

328 We thank all the members of our laboratory for their critical assistance and helpful discussions. This work is
329 supported by grants from the Natural Science Foundation of China (81671996 and 81871643) to E.K. and the
330 Natural Science Foundation of China (81971928) to X.Li.

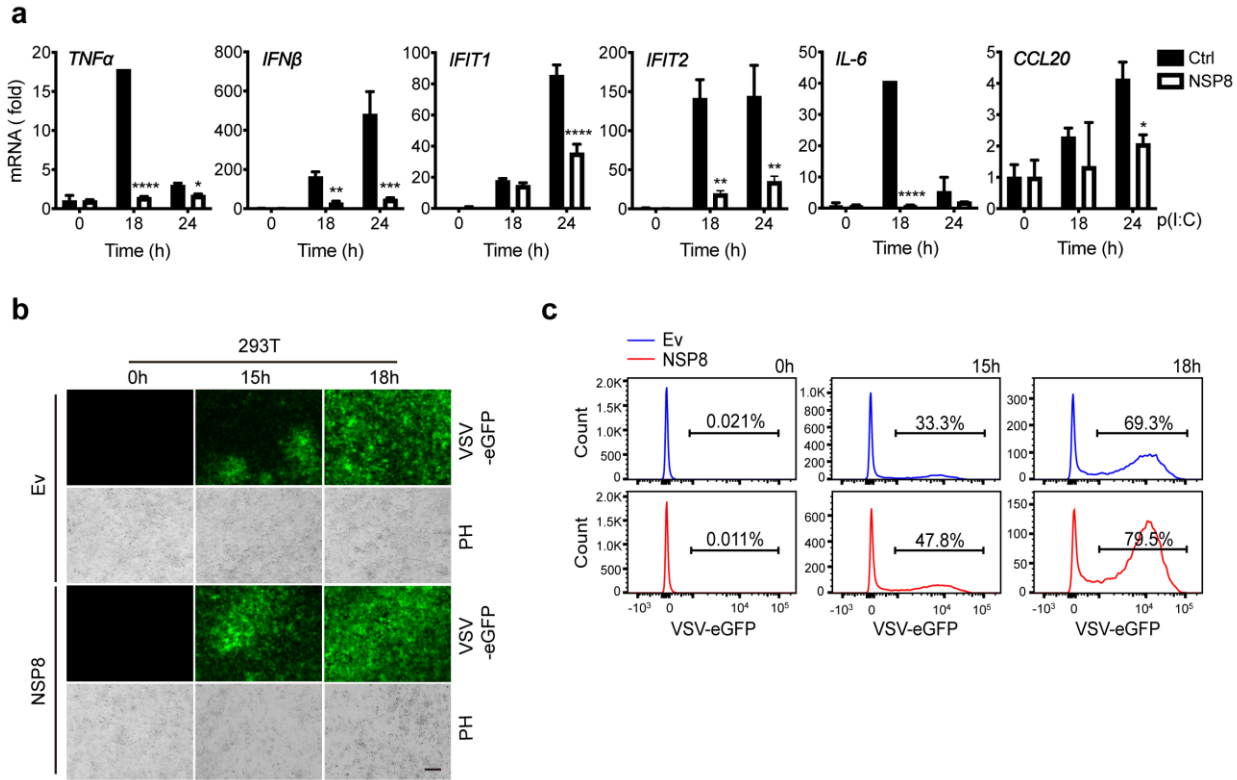
331

332

333 **Conflict of interest statement**

334 The authors declare no competing financial interest.

335



336

337

338

Figure 1. NSP8 inhibits the viral RNA-induced type I IFN signaling pathway.

339 a. HEK293T cells were transfected with a control vector (Ctrl) or *Flag-NSP* plasmids. Twenty-four hours post
 340 transfection, cells were treated with poly(I:C) (5 μ M) for the indicated time points and then subjected to RT-
 341 PCR analysis for *TNF- α* , *IFN- β* , *IFIT1*, *IFIT2*, *IL-6* and *CCL20* expression. Data are shown as the mean
 342 values \pm SD (n = 3). *, p < 0.0332; **, p < 0.0021; ***, p < 0.0002; ****, p < 0.0001; by Sidak's multiple
 343 comparisons test.

344 b. HEK293T cells were transfected with an empty vector or *Flag-NSP8*. Twenty-four hours post transfection,
 345 cells were infected with VSV-eGFP (MOI = 0.01) for the indicated time points and subjected to phase-
 346 contrast (PH) or fluorescence analyses. Scale bar, 15 μ m.

347 c. eGFP-positive cells were detected by flow cytometry. Numbers indicate the representative percentage of
 348 eGFP-positive cells of three independent experiments.

349

350

351

352

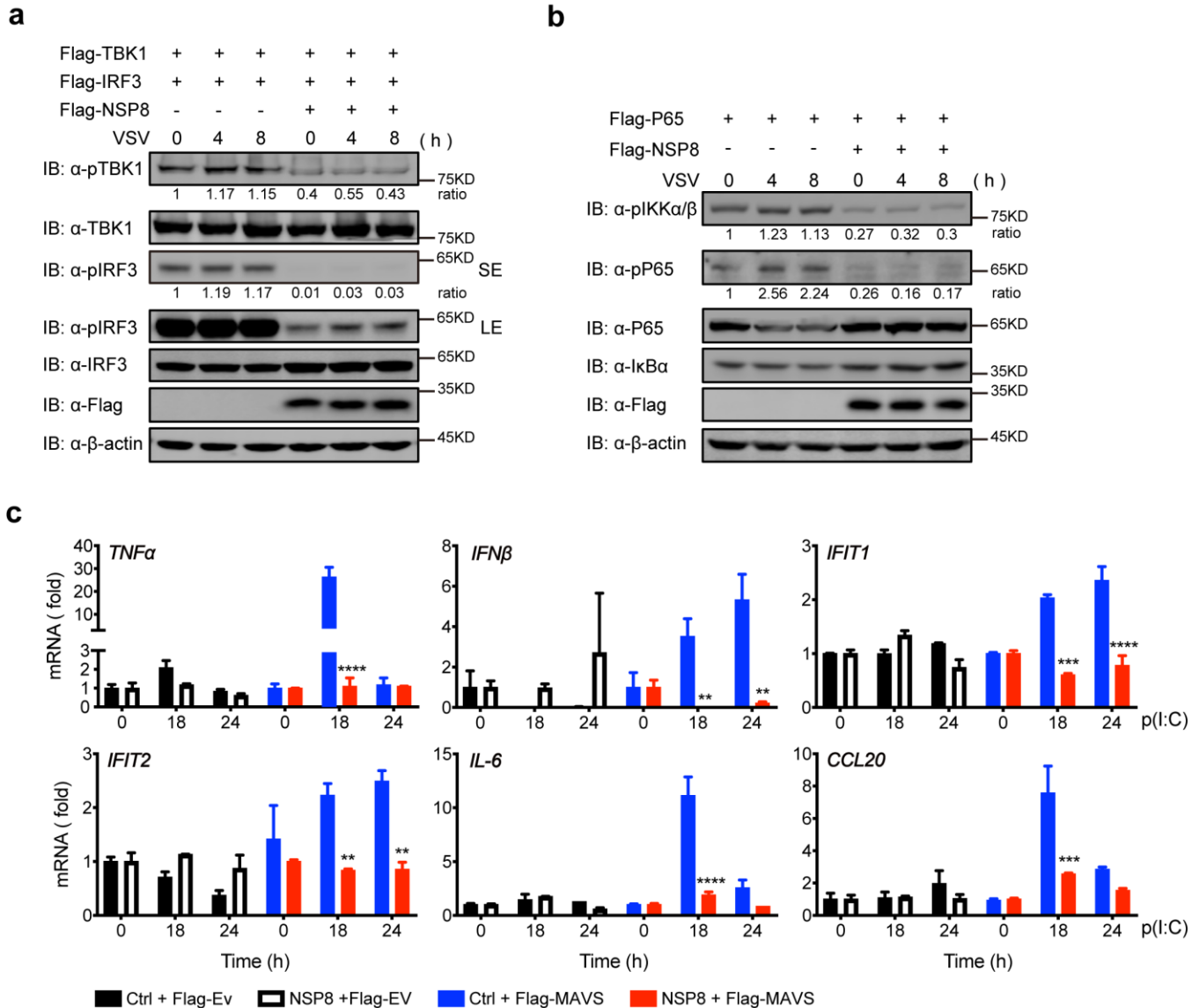
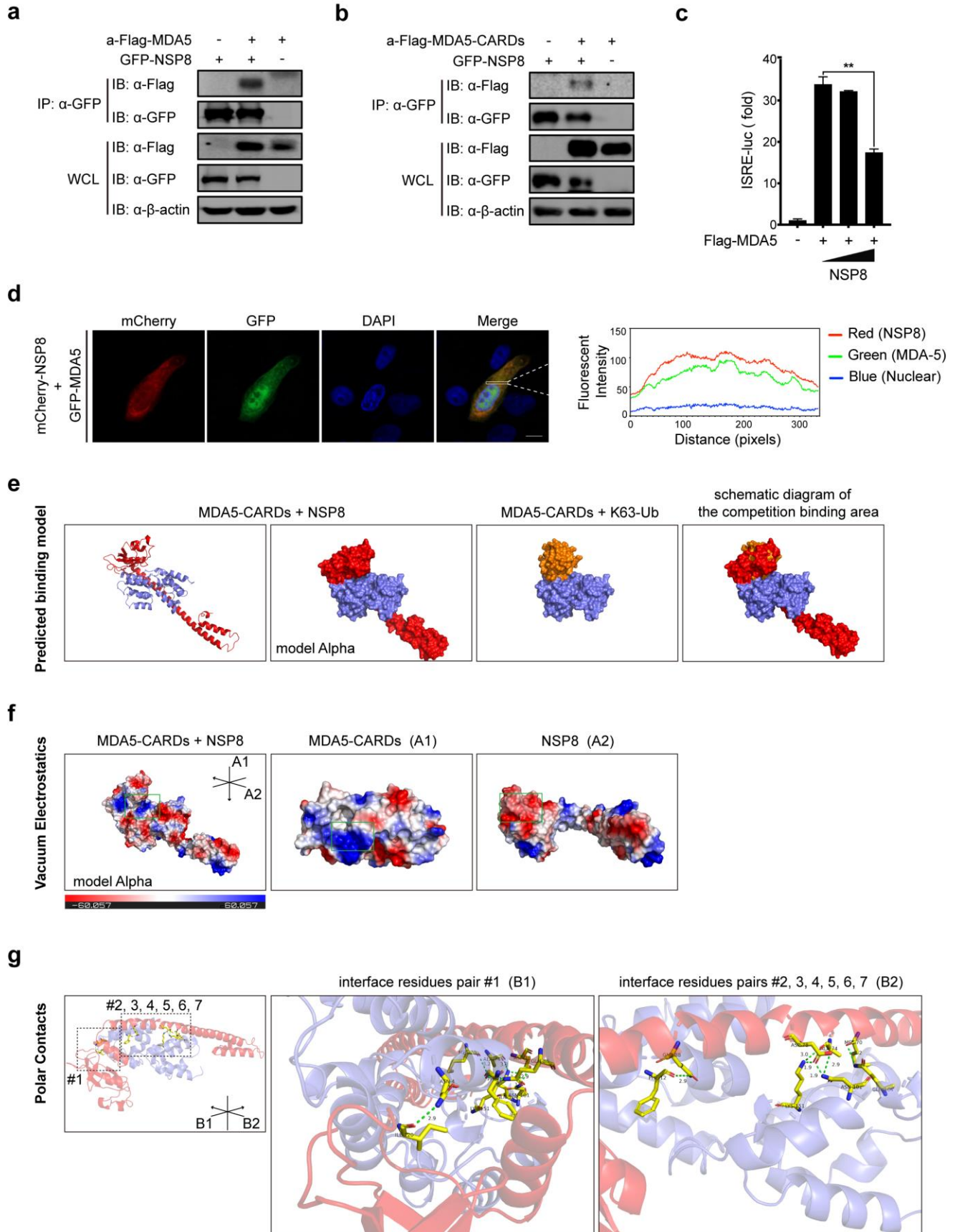


Figure 2. NSP8 inhibits the MAVS-dependent immune signaling pathway.

a-b. HEK293T cells were transfected with an empty vector or *Flag-NSP8* for 8 h and then transfected with *Flag-TBK1* and *Flag-IRF3* (a) or transfected with *Flag-p65* (b). Twenty-four hours post transfection, cells were infected with VSV-eGFP (MOI = 1) for the indicated time points and then harvested. Whole cell extracts were analyzed by immunoblotting as indicated. Representative images of three independent experiments are shown.

c. *MAVS* knockout HEK293T cells were cotransfected with *Flag-NSP8* and an empty vector or *Flag-MAVS*. Twenty-four hours post transfection, cells were treated with poly(I:C) (5 μg/ml) for the indicated time points, and then total RNA was extracted and subjected to RT-PCR analysis for *TNF-α*, *IFN-β*, *IFIT1*, *IFIT2*, *IL-6* and *CCL20* expression. The data are shown as the mean values ± SD (n = 3). *, p < 0.0332; **, p < 0.0021; ***, p < 0.0002; ****, p < 0.0001; by Sidak's multiple comparisons test.



366 **Figure 3. NSP8 interacts with MDA5 at the CARD domain.**

367 a-b. HEK293T cells were transfected with *GFP-NSP8* and full-length *Flag-MDA5* (a) or *Flag-MDA5-CARD* (b),
368 and after 36 h, the cells were collected and lysed. Then, cell lysates were subjected to coimmunoprecipitation
369 using anti-GFP beads, followed by immunoblotting with the indicated antibodies.

370 c. HEK293T cells were transfected with an empty vector or increasing amounts of *NSP8*-expressing plasmid
371 plus an *ISRE-luc* reporter and *MDA5*-expressing plasmids. Twenty-four hours post transfection, the cells were
372 collected, and then cell lysates were analyzed for ISRE-luc activity. The representative results of three
373 independent experiments are shown as the mean values \pm SD (n = 3).

374 d. HEK293T cells were cotransfected with mCherry-NSP8 and GFP-MDA5. Twenty-four hours post
375 transfection, the images were visualized by confocal microscopy analysis. Scale bar, 10 μ m. The colocalization
376 coefficient was determined by qualitative analysis of the fluorescence intensity of the selected area in Merge.

377 e-g. Computer-based prediction and structural modeling of the interaction of NSP8-MDA5 CARD domains.

378 e. Structural prediction of the MDA5-CARD-NSP8 interaction and MDA5-CARD linkage with K63-Ub. PDB
379 structures were input into ZDOCK Server for docking calculation separately. The predicted binding models of
380 MDA5 CARDS with NSP8 and MDA5 CARDS with K63-Ub were processed in PyMOL for demonstration. Model
381 alpha simulates the protein surface. Red chain, NSP8; violet chain, MDA5 CARDS; brown chain, K63-Ub.

382 f. Model alpha in (e) was subjected to vacuum electrostatics calculation in PyMOL. A1 and A2 indicate the
383 viewing angle in the green frame. The green frame indicates the contact area demonstrated in A1 and A2.
384 Scale bar indicates the range of vacuum electrostatics.

385 g. Polar contacts within interface of MDA5-CARD-USP8 were demonstrated with PyMOL. B1, B2 indicates
386 the viewing angle of dashed borders. #1, 2, 3, 4, 5, 6, 7 indicates paired residues. Paired residues were
387 highlighted with sticks model in yellow color. Green dashed lines indicate polar contacts between paired
388 residues, number besides dashed line indicates distance between two atoms connected (\AA).

389

390

391

392

393

394

395

396

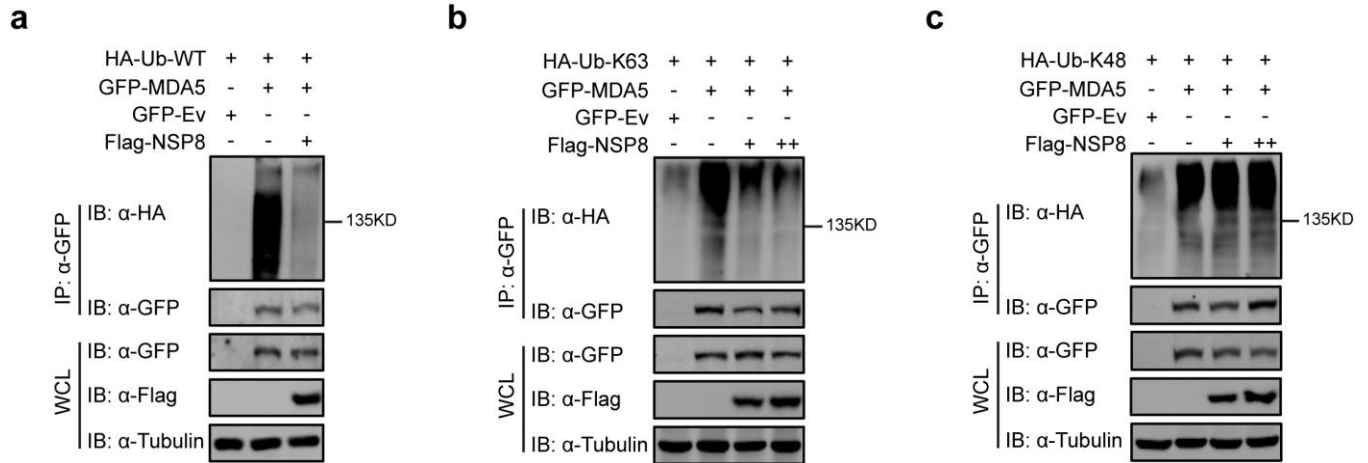
397

398

399

400

401



402

403

404

Figure 4. NSP8 suppresses K63-linked polyubiquitination of MDA5.

405

406

407

408

409

410

411

412

413

414

415

416

417

418

419

420

421

422

423

424

425

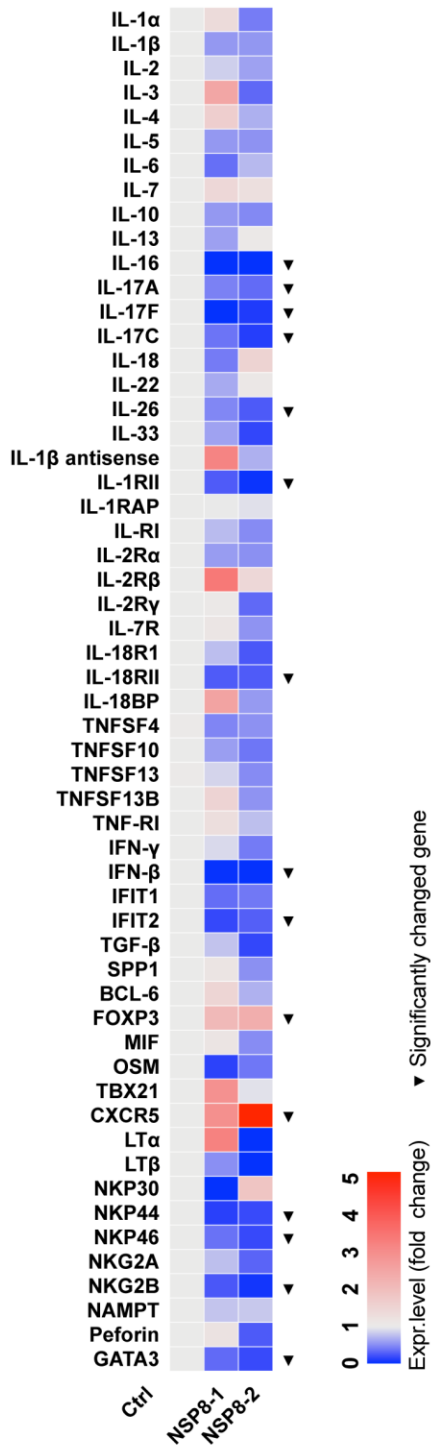
426

427

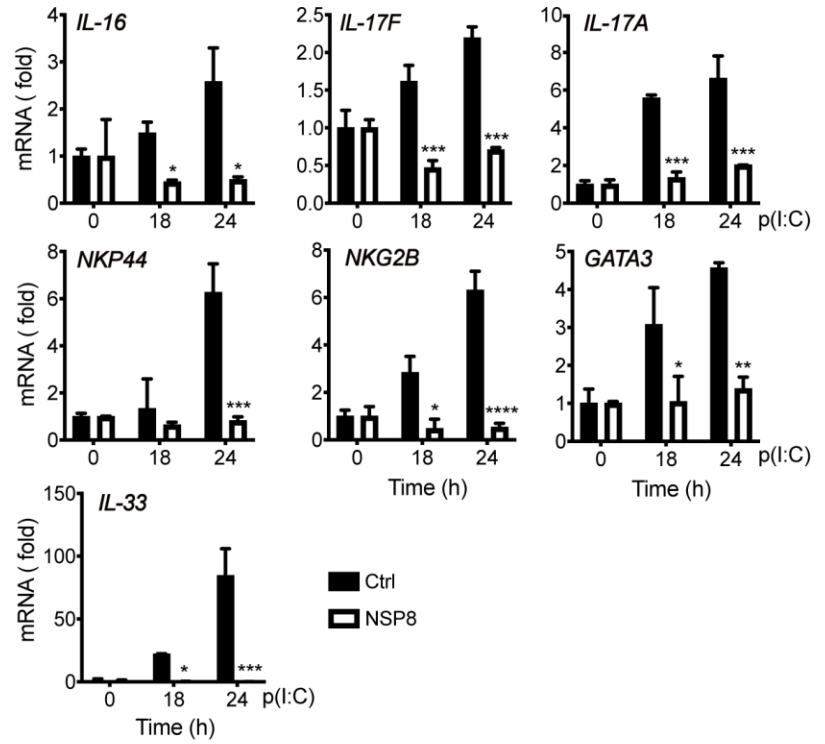
428

a-c. HEK293T cells were cotransfected with *HA-Ub-WT* (a), *HA-Ub-K63* (b) or *HA-Ub-K48* (c) and *GFP-MDA5* or *GFP*-tagged empty vector plus *Flag-NSP8*. Twenty hours post transfection, cells were treated with MG132 (5 μ M) for 4 h, and then cells were collected and lysed in 0.1% SDS-containing lysis buffer. Cell lysates were subjected to coimmunoprecipitation using anti-GFP beads, followed by immunoblotting analysis with the indicated antibodies. Representative images of three independent experiments are shown.

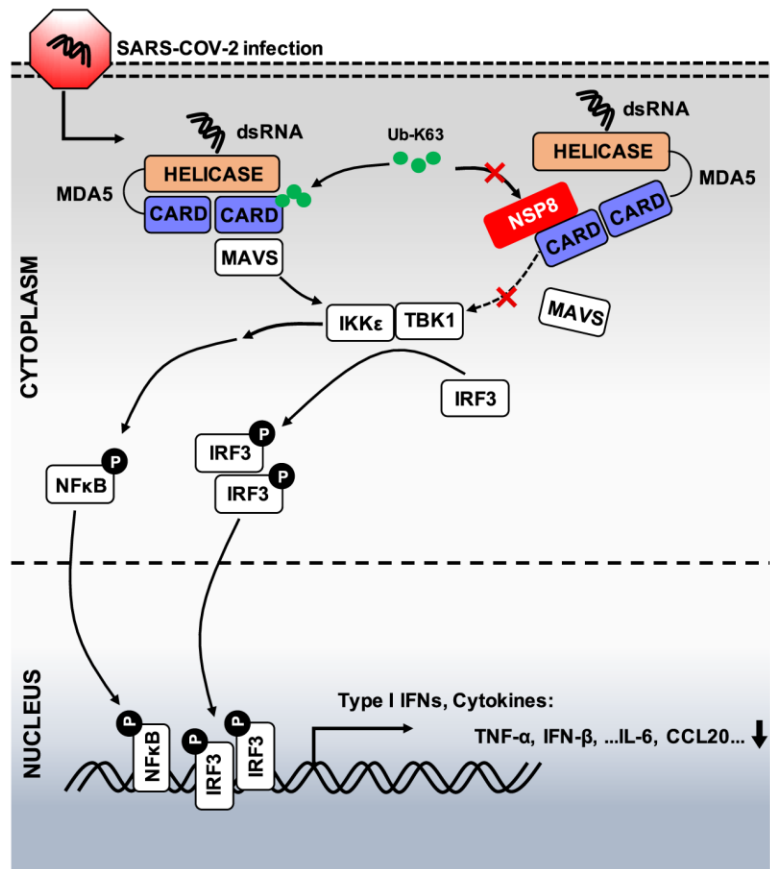
a



b



c



430
431
432
433
434
435
436
437
438
439
440
441
442
443
444
445
446
447
448
449
450
451
452
453
454
455
456
457
458
459
460
461
462
463
464
465

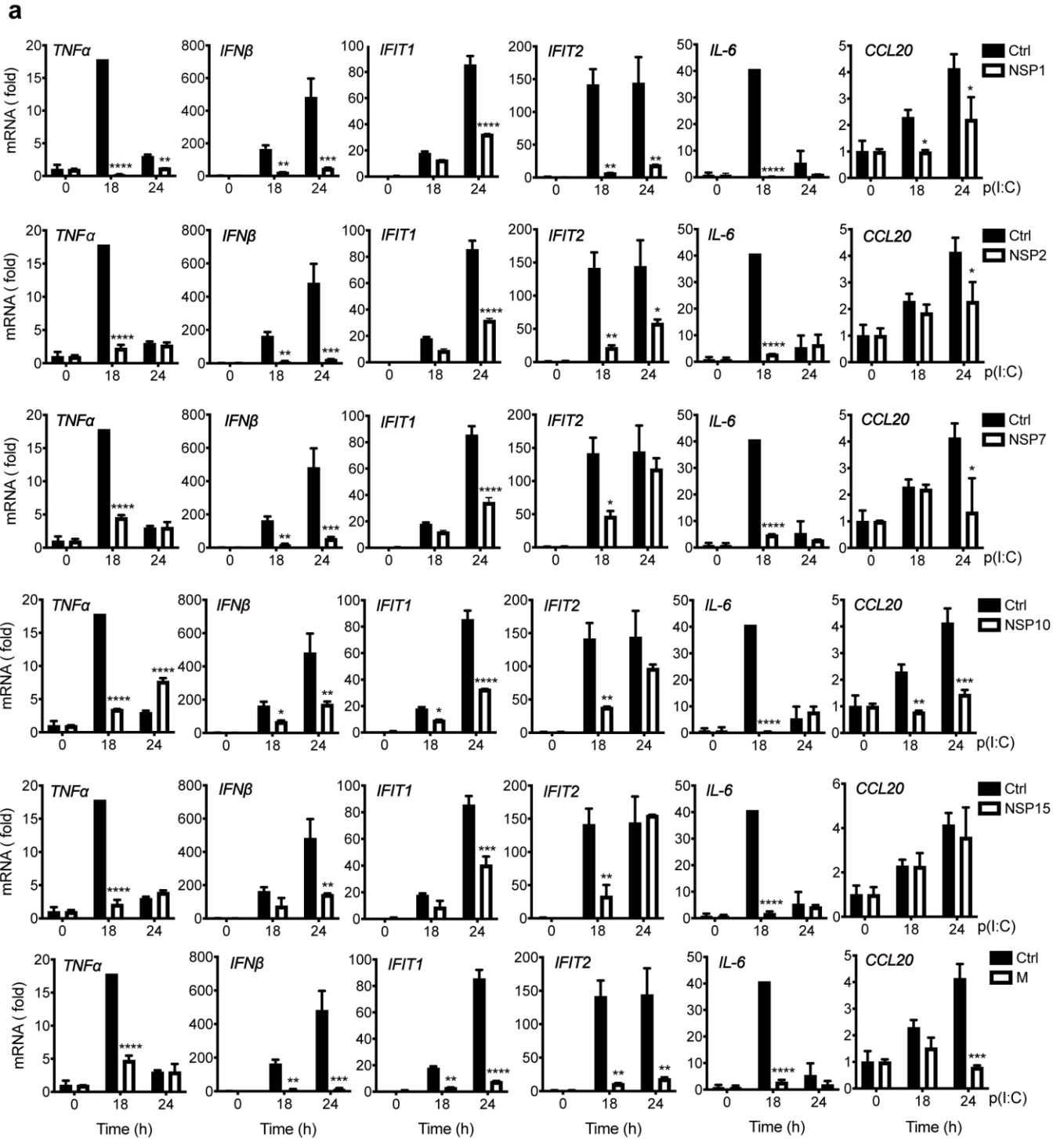
Figure 5. NSP8 decreases the expression of antiviral immune and inflammatory factors.

a. A549 cells were transfected with an empty vector or *Flag-NSP8*. Thirty-six hours post transfection, cells were collected, and total RNA was extracted and subjected to RT-PCR analysis for the expression of the indicated genes. “▼” indicates genes that were significantly changed in two independent *NSP8*-expressing samples.

b. A549 cells were transfected with an empty vector or *Flag-NSP8*. Twenty-four hours post transfection, cells were treated with poly(I:C) (5 µg/ml) for the indicated time points, and then total RNA was extracted and subjected to RT-PCR analysis of the expression of selected genes.

The data are shown as the mean values ± SD (n = 3). *, p < 0.0332; **, p < 0.0021; ***, p < 0.0002; ****, p < 0.0001; by Sidak’s multiple comparisons test.

c. Working model of SARS-CoV-2 NSP8 negatively regulating the MDA5-mediated type I IFN signaling pathway. NSP8 interacts with MDA5 and impairs its K63-linked polyubiquitination, thus inhibiting the phosphorylation of TBK1 and IRF3 and subsequently downregulating the production of type I IFNs, immune cytokines and inflammatory factors.



466

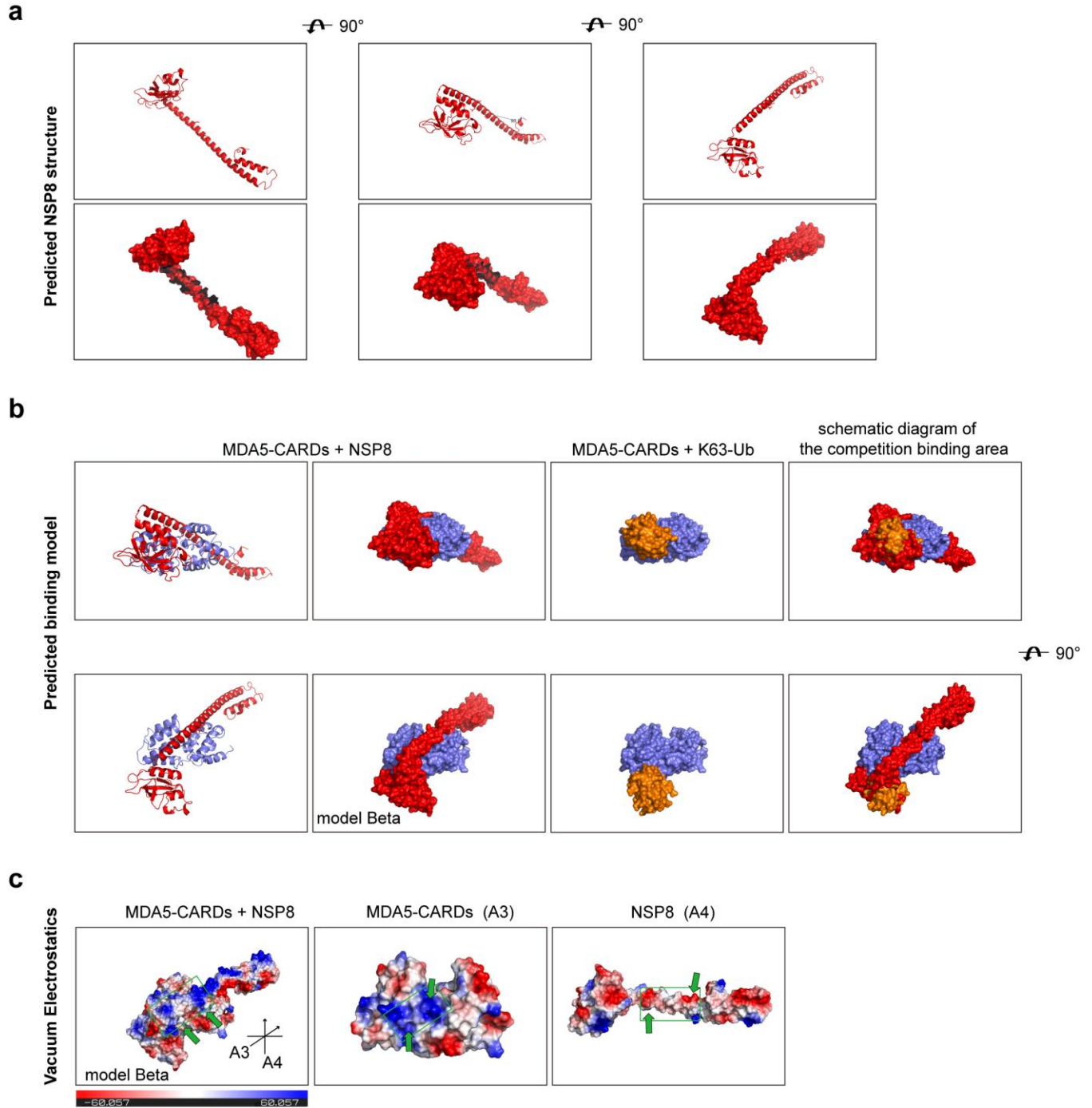
467

468

469

470

Supplementary Figure.1. Screening results of SARS-CoV-2 nonstructural proteins in the regulation of type I IFN signaling. HEK293T cells were transfected with empty vector (Ctrl) or Flag-NSP plasmids. Twenty-four hours post transfection, cells were treated with poly(I:C) (5 μ M) for the indicated time, and total RNA was subjected to RT-PCR analysis of TNF- α , IFN- β , IFIT1, IFIT2, IL-6 and CCL20 expression.



471

472

473

Supplementary Figure.2. Predicted structure of NSP8 and its binding with MDA5 CARDs

474 a. The PDB structure of NSP8 was processed in PyMOL. The cartoon structure and surface structure are
475 demonstrated.

476 b. PDB structure of MDA5 CARD with NSP8 and MDA5 CARD with K63-Ub. PDB structures were input into
477 the ZDOCK Server separately for docking calculations. The predicted binding models of MDA5 CARDs with

478 NSP8 and MDA5 CARDS with K63-Ub were processed in PyMOL for demonstration. Model alpha simulates
479 the protein surface. Red chain, NSP8; violet chain, MDA5 CARDS; brown chain, K63-Ub.

480 c. Model alpha in (b) was subjected to vacuum electrostatics calculation in PyMOL. A3 and A4 indicate the
481 viewing angle in the green frame. The green frame indicates the contact area demonstrated in A3 and A4. The
482 scale bar indicates the range of vacuum electrostatics.

483

484

485

486

487

488

489

490

491

492

493

494

495

496

497

498

499

500

501

502

503

504

505

506

507

508

509

510

511

512

513

<i>IL-1α</i>	forward	5'-TGATGTGACTGCCAAGATGAAG-3'	<i>TNFSF13</i>	forward	5'-CGAAAAGGAGAGCAGTGCTCA-3'
	reverse	5'-AGAGGAGGTTGGTCTCACTACC-3'		reverse	5'-GCCTAAGAGCTGGTTGCCACAT-3'
<i>IL-1β</i>	forward	5'-CCACAGACCTCCAGGAGAATG-3'	<i>TNFSF13B</i>	forward	5'-ACCACGCGGAGAAGCTGCCAG-3'
	reverse	5'-GTGCAGTTCAGTGATCGTACAGG-3'		reverse	5'-CTGCTGTTCTGACTGGAGTTGC-3'
<i>IL-2</i>	forward	5'-AGAACTCAAACCTCTGGAGGAAG-3'	<i>IFN-γ</i>	forward	5'-GAGTGTGGAGACCATCAAGGAAG-3'
	reverse	5'-GCTGTCTCATCAGCATATTCACAC-3'		reverse	5'-TGCTTTGCGTTGGACATTCAAGTC-3'
<i>IL-3</i>	forward	5'-AAGCAGCCACCTTTGCCTTTGCC-3'	<i>IFN-β</i>	forward	5'-CCTACAAAGAAGCAGCAA-30-3'
	reverse	5'-ACAGCCCTGTTGAATGCCTCCA-3'		reverse	5'-TCCTCAGGGATGTCAAAG-30-3'
<i>IL-4</i>	forward	5'-CCGTAACAGACATCTTTGCTGCC-3'	<i>IFIT1</i>	forward	5'-GCCTTGCTGAAGTGTGGAGAA-3'
	reverse	5'-GAGTGTCTTCTCATGGTGGCT-3'		reverse	5'-ATCCAGGCGATAGGCAGAGATC-3'
<i>IL-5</i>	forward	5'-GGAATAGCACACTGGAGATC-3'	<i>IFIT2</i>	forward	5'-GGAGCAGATTCTGAGCTTTGC-3'
	reverse	5'-CTCTCCGCTTTCTTCTCCACAC-3'		reverse	5'-GGATGAGGCTCCAGACTCCAA-3'
<i>IL-6</i>	forward	5'-AGACAGCCACTCACCTTTCAG-3'	<i>TGF-β</i>	forward	5'-TACCTGAACCCGTGTTGCTCTC-3'
	reverse	5'-TTCTGCCAGTGCCTCTTTGCTG-3'		reverse	5'-GTTGCTGAGGTATGCCAGGAA-3'
<i>IL-7</i>	forward	5'-GACAGCATGAAAGAAATGGTAGC-3'	<i>SPP1</i>	forward	5'-CGAGGTGATAGTGTGGTTTATGG-3'
	reverse	5'-CAACTTGCAGCAGCACGGAAT-3'		reverse	5'-GCACCATTCAACTCTCGCTTTC-3'
<i>IL-10</i>	forward	5'-TCTCCGAGATGCCCTCAGCAGA-3'	<i>BCL-6</i>	forward	5'-CATGCAGAGATGTGCCTCCACA-3'
	reverse	5'-TCAGACAAGGCTTGCAACCCA-3'		reverse	5'-TCAGAGAAGCGGCAGTCACACT-3'
<i>IL-13</i>	forward	5'-ACGGTCATTGCTCTCACTTGCC-3'	<i>FOXP3</i>	forward	5'-GGCACAATGTCTCCTCCAGAGA-3'
	reverse	5'-CTGTGAGTTGATGCTCCATACC-3'		reverse	5'-CAGATGAAGCCTTGGTCACTGC-3'
<i>IL-16</i>	forward	5'-TTGGACACAGGTTCTCGCTCA-3'	<i>MIF</i>	forward	5'-AGAACCCTCTACAGCAAGCT-3'
	reverse	5'-AGCAGGGAGATAACGGACTGAC-3'		reverse	5'-GGAGTTGTTCCAGCCACATTG-3'
<i>IL-17A</i>	forward	5'-CGGACTGTGATGGTCAACCTGA-3'	<i>OSM</i>	forward	5'-GAAAGAGTACCGCTGCTCCTT-3'
	reverse	5'-GCACTTTGCTCCAGATCACA-3'		reverse	5'-CTCTCAGTTTAGAACATCCAGG-3'
<i>IL-17F</i>	forward	5'-AACCAGCGGTTTCCATGTCAC-3'	<i>TBX21</i>	forward	5'-ATTGCCGTGACTGCCTACCAGA-3'
	reverse	5'-GAGCATTGATGCAGCCCAAGTTC-3'		reverse	5'-GGAATTGACAGTTGGTCCAGG-3'
<i>IL-17C</i>	forward	5'-GCCCTCAGCTACGACCCAGTG-3'	<i>CXCR5</i>	forward	5'-TGAAGTCCGCACTGACCTGTC-3'
	reverse	5'-AGCTTCTGTGGATAGCGGCTCT-3'		reverse	5'-GAGGTGGCATTCTGACTCAG-3'
<i>IL-18</i>	forward	5'-GATAGCCAGCCTAGAGGTATGG-3'	<i>LTα</i>	forward	5'-ACACCTCAGCTGCCAGACTG-3'
	reverse	5'-CCTTGATGTTATCAGGAGATTCA-3'		reverse	5'-TCCGTGTTGCTCTCCAGAGCA-3'
<i>IL-22</i>	forward	5'-GTTCCAGCCTTATATGCAGGAGG-3'	<i>LTβ</i>	forward	5'-GGTTTCAGAAGCTGCCAGAGGA-3'
	reverse	5'-GCACATTCTCTGGATATGCAGG-3'		reverse	5'-CGTCAGAAACGCTGTTCTTC-3'
<i>IL-26</i>	forward	5'-GGAAGACGTTTTGGTCAACTGC-3'	<i>NKP30</i>	forward	5'-CCAGCATCTACGTGTGCAGAGT-3'
	reverse	5'-CTCTCTAGCTGATGAAGCACAGG-3'		reverse	5'-GCATAGAATCCAGCCGAAGGA-3'
<i>IL-33</i>	forward	5'-GCCTGTCAACAGCAGTCTACTG-3'	<i>NKP44</i>	forward	5'-CTGAGTCTCCATCTACCATCCC-3'
	reverse	5'-TGTGCTTAGAGAAGCAAGATACTC-3'		reverse	5'-TCTTGCTACGAGGAGTCCACA-3'
<i>IL-1RII</i>	forward	5'-GGCTATTACCGCTGTGCTCGA-3'	<i>NKP46</i>	forward	5'-CAGCAACTTGTGGATCTGGTG-3'
	reverse	5'-GAGAAGCTGATATGGTCTGAGG-3'		reverse	5'-AGACGGCAGTAGAAGGTCACCT-3'
<i>IL-1RAP</i>	forward	5'-CTGAGGATCTAAGCGCAGCTA-3'	<i>NKG2A</i>	forward	5'-GCCTCTGTGGTAACGATAGTTGT-3'
	reverse	5'-AGCAGGACTGTGGCTCCAAAAC-3'		reverse	5'-ATCCACTCTCAGGACAATGGC-3'
<i>IL-2Ra</i>	forward	5'-GAGACTTCTGCCTCGTCACAA-3'	<i>NAMPT</i>	forward	5'-AGGGTTACAAGTTGCTGCCACC-3'
	reverse	5'-GATCAGCAGGAAAACACAGCCG-3'		reverse	5'-CTCCACCAGAACCGAAGGCAAT-3'
<i>IL-2Rβ</i>	forward	5'-GGTGAACCAAACCTGTGAGCT-3'	<i>Peforin</i>	forward	5'-ACTCACAGGCAGCCAACTTTGC-3'
	reverse	5'-GGTGACGATGTCAACTGTGGTC-3'		reverse	5'-CTCTTGAAGTCAGGGTGCAGCG-3'
<i>IL-7R</i>	forward	5'-ATCGCAGCACTCACTGACCTGT-3'	<i>GATA3</i>	forward	5'-ACCACAACCACACTCTGGAGGA-3'
	reverse	5'-TCAGGCACTTACCTCCACGAG-3'		reverse	5'-TCGGTTCTGGTCTGGATGCCT-3'
<i>IL-18R1</i>	forward	5'-GGAGGCACAGACACCAAAGCT-3'	<i>TNFα</i>	forward	5'-CTCTTCTGCCTGCTGCACCTTG-3'
	reverse	5'-AGGCACACTACTGCCACCAAGA-3'		reverse	5'-ATGGGCTACAGGCTTGTCACTC-3'
<i>IL-18BP</i>	forward	5'-GTGTCCAGCATTGGAAGTGACC-3'	<i>IL-6</i>	forward	5'-AGACAGCCACTCACCTTTCAG-3'
	reverse	5'-GGAGGTGCTCAATGAAGGAACC-3'		reverse	5'-TTCTGCCAGTGCCTCTTTGCTG-3'
<i>TNFSF4</i>	forward	5'-CCTACATCTGCCTGCCTTCTC-3'	<i>CCL20</i>	forward	5'-AAGTTGTCTGTGTGCCAAATCC-3'
	reverse	5'-TGATGACTGAGTTGTTCTGCACC-3'		reverse	5'-CCATTCCAGAAAAGCCACAGTTT-3'
<i>TNFSF10</i>	forward	5'-TGGCAACTCCGTCAGCTCGTTA-3'			
	reverse	5'-AGCTGCTACTCTCTGAGGACCT-3'			

515 **Supplementary Table.1. The primer pairs of the RT-PCR array.**
516 The sequences of primer pairs used in the RT-PCR array (Fig.5a) are listed.
517

518 **References**

- 519 1 Fehr, A. R., Channappanavar, R. & Perlman, S. Middle East Respiratory Syndrome: Emergence of a Pathogenic
520 Human Coronavirus. *Annual review of medicine* **68**, 387-399, doi:10.1146/annurev-med-051215-031152
521 (2017).
- 522 2 Channappanavar, R. *et al.* Dysregulated Type I Interferon and Inflammatory Monocyte-Macrophage
523 Responses Cause Lethal Pneumonia in SARS-CoV-Infected Mice. *Cell host & microbe* **19**, 181-193,
524 doi:10.1016/j.chom.2016.01.007 (2016).
- 525 3 Chen, Y., Liu, Q. & Guo, D. Emerging coronaviruses: Genome structure, replication, and pathogenesis. *Journal*
526 *of medical virology* **92**, 418-423, doi:10.1002/jmv.25681 (2020).
- 527 4 Xiong, Y. *et al.* Transcriptomic characteristics of bronchoalveolar lavage fluid and peripheral blood
528 mononuclear cells in COVID-19 patients. *Emerging microbes & infections* **9**, 761-770,
529 doi:10.1080/22221751.2020.1747363 (2020).
- 530 5 Huang, C. *et al.* Clinical features of patients infected with 2019 novel coronavirus in Wuhan, China. *Lancet*
531 **395**, 497-506, doi:10.1016/s0140-6736(20)30183-5 (2020).
- 532 6 Chen, N. *et al.* Epidemiological and clinical characteristics of 99 cases of 2019 novel coronavirus pneumonia
533 in Wuhan, China: a descriptive study. *Lancet (London, England)* **395**, 507-513, doi:10.1016/s0140-
534 6736(20)30211-7 (2020).
- 535 7 Akira, S. & Hemmi, H. Recognition of pathogen-associated molecular patterns by TLR family. *Immunology*
536 *letters* **85**, 85-95, doi:10.1016/s0165-2478(02)00228-6 (2003).
- 537 8 Theofilopoulos, A. N., Baccala, R., Beutler, B. & Kono, D. H. Type I interferons (alpha/beta) in immunity and
538 autoimmunity. *Annual review of immunology* **23**, 307-336, doi:10.1146/annurev.immunol.23.021704.115843
539 (2005).
- 540 9 Huang, C. *et al.* SARS coronavirus nsp1 protein induces template-dependent endonucleolytic cleavage of
541 mRNAs: viral mRNAs are resistant to nsp1-induced RNA cleavage. *PLoS pathogens* **7**, e1002433,
542 doi:10.1371/journal.ppat.1002433 (2011).
- 543 10 Tanaka, T., Kamitani, W., DeDiego, M. L., Enjuanes, L. & Matsuura, Y. Severe acute respiratory syndrome
544 coronavirus nsp1 facilitates efficient propagation in cells through a specific translational shutoff of host

- 545 mRNA. *Journal of virology* **86**, 11128-11137, doi:10.1128/jvi.01700-12 (2012).
- 546 11 Frieman, M., Ratia, K., Johnston, R. E., Mesecar, A. D. & Baric, R. S. Severe acute respiratory syndrome
547 coronavirus papain-like protease ubiquitin-like domain and catalytic domain regulate antagonism of IRF3
548 and NF-kappaB signaling. *Journal of virology* **83**, 6689-6705, doi:10.1128/jvi.02220-08 (2009).
- 549 12 Lei, Y. *et al.* MAVS-mediated apoptosis and its inhibition by viral proteins. *PloS one* **4**, e5466,
550 doi:10.1371/journal.pone.0005466 (2009).
- 551 13 Züst, R. *et al.* Ribose 2'-O-methylation provides a molecular signature for the distinction of self and non-self
552 mRNA dependent on the RNA sensor Mda5. *Nature immunology* **12**, 137-143, doi:10.1038/ni.1979 (2011).
- 553 14 Chen, Y. *et al.* Biochemical and structural insights into the mechanisms of SARS coronavirus RNA ribose 2'-
554 O-methylation by nsp16/nsp10 protein complex. *PLoS pathogens* **7**, e1002294,
555 doi:10.1371/journal.ppat.1002294 (2011).
- 556 15 Decroly, E. *et al.* Crystal structure and functional analysis of the SARS-coronavirus RNA cap 2'-O-
557 methyltransferase nsp10/nsp16 complex. *PLoS pathogens* **7**, e1002059, doi:10.1371/journal.ppat.1002059
558 (2011).
- 559 16 Huang, S. H. *et al.* Phage display technique identifies the interaction of severe acute respiratory syndrome
560 coronavirus open reading frame 6 protein with nuclear pore complex interacting protein NPIP3 in
561 modulating Type I interferon antagonism. *Journal of microbiology, immunology, and infection = Wei mian yu*
562 *gan ran za zhi* **50**, 277-285, doi:10.1016/j.jmii.2015.07.002 (2017).
- 563 17 Shi, C. S. *et al.* SARS-coronavirus open reading frame-9b suppresses innate immunity by targeting
564 mitochondria and the MAVS/TRAF3/TRAF6 signalosome. *J Immunol* **193**, 3080-3089,
565 doi:10.4049/jimmunol.1303196 (2014).
- 566 18 Canton, J. *et al.* MERS-CoV 4b protein interferes with the NF-κB-dependent innate immune response during
567 infection. *PLoS pathogens* **14**, e1006838, doi:10.1371/journal.ppat.1006838 (2018).
- 568 19 Thoms, M. *et al.* Structural basis for translational shutdown and immune evasion by the Nsp1 protein of
569 SARS-CoV-2. *Science*, doi:10.1126/science.abc8665 (2020).
- 570 20 Jiang, X. *et al.* Ubiquitin-induced oligomerization of the RNA sensors RIG-I and MDA5 activates antiviral
571 innate immune response. *Immunity* **36**, 959-973, doi:10.1016/j.immuni.2012.03.022 (2012).

- 572 21 Zhao, C. *et al.* The E3 Ubiquitin Ligase TRIM40 Attenuates Antiviral Immune Responses by Targeting MDA5
573 and RIG-I. *Cell reports* **21**, 1613-1623, doi:10.1016/j.celrep.2017.10.020 (2017).
- 574 22 Fischer, H., Tschachler, E. & Eckhart, L. Pangolins Lack IFIH1/MDA5, a Cytoplasmic RNA Sensor That Initiates
575 Innate Immune Defense Upon Coronavirus Infection. *Frontiers in immunology* **11**, 939,
576 doi:10.3389/fimmu.2020.00939 (2020).
- 577 23 Liu, H. M. *et al.* Regulation of Retinoic Acid Inducible Gene-I (RIG-I) Activation by the Histone Deacetylase 6.
578 *EBioMedicine* **9**, 195-206, doi:10.1016/j.ebiom.2016.06.015 (2016).
- 579 24 Gupta, S. *et al.* Herpesvirus deconjugases inhibit the IFN response by promoting TRIM25 autoubiquitination
580 and functional inactivation of the RIG-I signalosome. *PLoS pathogens* **14**, e1006852,
581 doi:10.1371/journal.ppat.1006852 (2018).
- 582 25 Riedl, W. *et al.* Zika Virus NS3 Mimics a Cellular 14-3-3-Binding Motif to Antagonize RIG-I- and MDA5-
583 Mediated Innate Immunity. *Cell host & microbe* **26**, 493-503.e496, doi:10.1016/j.chom.2019.09.012 (2019).
- 584 26 Cui, J. *et al.* NLRP4 negatively regulates type I interferon signaling by targeting the kinase TBK1 for
585 degradation via the ubiquitin ligase DTX4. *Nature immunology* **13**, 387-395, doi:10.1038/ni.2239 (2012).
- 586 27 Biasini, M. *et al.* SWISS-MODEL: modelling protein tertiary and quaternary structure using evolutionary
587 information. *Nucleic acids research* **42**, W252-258, doi:10.1093/nar/gku340 (2014).
- 588 28 Pierce, B. G. *et al.* ZDOCK server: interactive docking prediction of protein-protein complexes and symmetric
589 multimers. *Bioinformatics (Oxford, England)* **30**, 1771-1773, doi:10.1093/bioinformatics/btu097 (2014).
- 590